doi:10.1016/j.jmb.2009.07.071 J. Mol. Biol. (2009) 392, 1020–1032

JMB

Available online at www.sciencedirect.com

ScienceDirect

ELSEVIER

The ATPase Cycle of PcrA Helicase and Its Coupling to Translocation on DNA

Christopher P. Toseland, Maria M. Martinez-Senac, Andrew F. Slatter and Martin R. Webb*

MRC National Institute for Medical Research, The Ridgeway, Mill Hill, London NW7 1AA, UK

Received 25 June 2009; received in revised form 22 July 2009; accepted 23 July 2009
Available online 30 July 2009

The superfamily 1 bacterial helicase PcrA has a role in the replication of certain plasmids, acting with the initiator protein (RepD) that binds to and nicks the double-stranded origin of replication. PcrA also translocates single-stranded DNA with discrete steps of one base per ATP hydrolyzed. Individual rate constants have been determined for the DNA helicase PcrA ATPase cycle when bound to either single-stranded DNA or a double-stranded DNA junction that also has RepD bound. The fluorescent ATP analogue 2′(3′)-*O*-(*N*-methylanthraniloyl)ATP was used throughout all experiments to provide a complete ATPase cycle for a single nucleotide species. Fluorescence intensity and anisotropy stopped-flow measurements were used to determine rate constants for binding and release. Quenched-flow measurements provided the kinetics of the hydrolytic cleavage step. The fluorescent phosphate sensor MDCC-PBP was used to measure phosphate release kinetics. The chemical cleavage step is the rate-limiting step in the cycle and is essentially irreversible and would result in the bound ATP complex being a major component at steady state. This cleavage step is greatly accelerated by bound DNA, producing the high activation of this protein compared to the protein alone. The data suggest the possibility that ADP is released in two steps, which would result in bound ADP also being a major intermediate, with bound ADP·P_i being a very small component. It therefore seems likely that the major transition in structure occurs during the cleavage step, rather than P_i release. ATP rebinding could then cause reversal of this structural transition. The kinetic mechanism of the PcrA ATPase cycle is very little changed by potential binding to RepD, supporting the idea that RepD increases the processivity of PcrA by increasing affinity to DNA rather than affecting the enzymatic properties *per se*.

Edited by D. E. Draper

Keywords: DNA helicase; ATPase; kinetics; fluorescence; plasmid replication

Introduction

DNA helicases are ubiquitous motor proteins involved in many aspects of DNA processing such as replication, recombination, and repair. Many enzymes are identified as helicases on the basis of conserved sequence motifs but are involved in more diverse processes such as Holliday junction progression and the processing of stalled replication forks.[1,2] Furthermore, proteins with these motifs may be DNA translocases rather than have helicase activity.[3] An important feature of helicases is that they couple the energy of nucleoside triphosphate, generally ATP, hydrolysis to their translocation, and/or strand separation activity.

PcrA helicase is an essential protein of gram-positive bacteria, where it has a role in DNA repair

*Corresponding author. E-mail address: mwebb@nimr.mrc.ac.uk.

Present address: M. M. Martinez-Senac, Universidad Católica San Antonio Murcia, Campus de los Jerónimos s/n, Guadalupe 30107, Murcia, Spain.

Abbreviations used: ssDNA, single-stranded DNA; dsDNA, double-stranded DNA; MDCC-PBP, phosphate binding protein (A197C) from *Escherichia coli*, labeled with MDCC (*N*-[2-(1-maleimidyl)ethyl]-7-diethylaminocoumarin-3-carboxamide); mantATP, 2′(3′)-*O*-(*N*-methylanthraniloyl)ATP; FRET, Förster resonance energy transfer; EDTA, ethylenediaminetetraacetic acid.

and rolling-circle replication of some plasmids. In the latter case, PcrA catalyzes the plasmid DNA unwinding.[4] Its helicase activity and processivity are greatly increased by the plasmid unwinding initiation factor RepD.[5] On its own, PcrA is a poor helicase with difficulty separating short lengths of duplex.[5,6] The helicase activity can be enhanced by having several PcrA molecules bound to the DNA whereby the dissociation of the first PcrA will allow the second to move in to its place.[6,7] In this way, the train of PcrA molecules can unwind a stretch of duplex DNA, in a way proposed for other helicases.[8,9] PcrA is a member of helicase superfamily 1 and is closely related to Rep, UvrD, and RecB, well-studied helicases from gram-negative bacteria. Structural and biochemical analysis of *Bacillus stearothermophilus* PcrA supports an "inchworm" mechanism to translocate DNA and separate the complementary strands in a 3′- to 5′-direction.[10–14] More recently, high-resolution structures of UvrD in different nucleotide states have added to our understanding of structural transitions for these related helicases.[15] The PcrA core subdomains 1A and 2A bind single-stranded DNA (ssDNA*) bases in pockets that open and close with conformational changes resulting from ATP binding and hydrolysis. ATP binding causes the pocket in domain 2A to close, binding the ssDNA, while the pockets in domain 1A open, releasing ssDNA. At the same time, the two domains move closer together. Upon ATP hydrolysis, the pockets in 1A close, binding ssDNA, and the pockets in 2A open, releasing ssDNA. The domains also move apart, causing the ssDNA to be pulled along the DNA binding channel relative to domain 2A, translocating the DNA. The motor hydrolyzes one ATP molecule per one base movement, whether the protein is translocating ssDNA or unwinding double-stranded DNA (dsDNA).[16,17]

In order to understand the mechanochemical coupling fully, we have analyzed the kinetic mechanism of the ATPase cycle for *B. stearothermophilus* PcrA. Different steps in the cycle require use of different methods to probe the kinetics. Techniques include use of signals from fluorescent ATP analogues, phosphate–water oxygen exchange, and quenched flow. In particular, the complete cycle was measured using the fluorescent analogue mantATP [2′(3′)-*O*-(*N*-methylanthraniloyl)ATP] to provide a consistent view of the cycle, as some rate constants are not readily accessible with the natural ATP substrate. The experimental approach allows us to define almost all individual rate constants in the ATPase cycle for this analogue. Where possible, comparison is made with the unmodified nucleotide, although not all steps can be readily studied in that case. The study shows that the ATP cleavage step is rate limiting during ssDNA translocation. DNA stimulates ATPase activity by more than 100-fold, largely through direct activation of the cleavage step. Data suggest that ADP is released in multiple steps, following rapid phosphate release. This, in turn, implies conformational changes within the cycle that may be related to the two states seen in the crystal structures.[10,13] Measurements were also done with the plasmid replication initiator protein RepD present to determine whether the ATPase cycle is modulated significantly, if PcrA is interacting with that protein. Given the high level of homology among helicases, the analysis of the PcrA ATPase cycle provides a foundation for further helicase studies.

Results

In order to understand how the ATPase cycle relates to the function and movement of PcrA, it is important to measure individual, elementary steps. We start by reporting data for PcrA on ssDNA, considered by using the simplest possible scheme that does not contain any extra steps for conformational changes, translocation, and so forth (Fig. 1a). This scheme also does not include initial PcrA binding to DNA, which was addressed previously.[18] Measurements described here start with PcrA prebound to DNA, except where stated. For some steps where possible, measurements were made with unmodified ATP for comparison with mantATP. Measurements are also reported for the ATPase cycle in the absence of DNA, to determine which steps are modulated by DNA. We also describe how the ATPase cycle is affected when PcrA is bound together with RepD on a dsDNA junction containing part of the double-stranded origin of replication *ori*D.

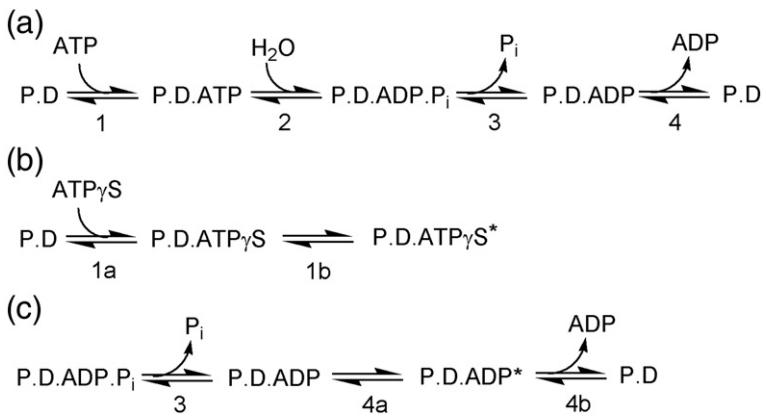

Fig. 1. ATPase mechanistic schemes. (a) Minimal mechanism for ATP hydrolysis by PcrA (P) with ssDNA (D). Steps are numbered, such that step n has forward and reverse rate constants, respectively, and equilibrium constant, K_n (k_{+n}/k_{-n}). (b) Two-step binding scheme for mantATPγS. (c) Two-step dissociation scheme for diphosphate release.

Table 1. Steady-state ATPase kinetics of PcrA

(a)

Nucleotide	k_{cat} (s^{-1})	±SE (s^{-1})	K_m (μM)	±SE (μM)
ATP	16.9	3	3.5	0.5
ATP (no DNA)	0.3	0.1	5	2
mantATP	17.2	2.3	2.6	0.4
mantATP (no DNA)	0.1	0.1	6	3.5

(b)

Nucleotide	K_i (μM)	±SE (μM)
ADP	>400	—
ATPγS	1.5	0.2
AMPPNP	195	8
mantADP	9.5	2
mantATPγS	3.6	1.5
mantAMPPNP	261	13

(c)

DNA	Vary [ATP]		Vary [DNA]	
dT_n	k_{cat} (s^{-1})	K_m (μM)	k_{cat} (s^{-1})	K_m (nM)
10	5.4	1.3	8.3	395
20	10.5	2	13.7	105
30	16.9	3.5	22	100
40	24.3	5.2	17.9	56

All measurements were carried out at 20 °C in the presence of 10 μM MDCC-PBP in buffer containing 50 mM Tris–HCl, pH 7.5, 150 mM NaCl, and 3 mM $MgCl_2$. (a) Determination of k_{cat} and K_m for nucleoside triphosphate used 2 nM PcrA and 0.5 μM dT_{30} with varying nucleotide concentration. (b) Competitive inhibition experiments to determine K_i for non-hydrolyzable nucleotides, using 10 nM PcrA, 100 nM dT_{20}, and 10 μM ATP and varying inhibitor concentration. (c) Determination of k_{cat} and K_m for DNA substrates, using 2 nM PcrA and 10 μM ATP with varying concentrations of oligonucleotides.

Steady-state ATPase rate measurements

Before describing measurement of individual processes in the ATPase cycle, steady-state ATPase measurements were made to gain an overall assessment of the reaction and the affinities of various nucleotides.

The inorganic phosphate (P_i) biosensor MDCC-PBP[19] was used to measure steady-state ATP hydrolysis. This produced a sensitive assay that could be used with low concentrations of ATP and low extents of reaction to circumvent some of the problems of alternative, coupled enzyme assays. Addition of multiple assay components in such coupled assays may make it difficult to ensure that the reaction of interest is not affected by the additions and that the rate observed is solely that of the ATPase. In any case, an inherent limitation of steady-state measurements is that the calculated rate constants are dependent on the percentage activity of the enzyme. In this case, PcrA activity may vary from batch to batch. However, steady-state assays are useful to assess the relative activity and affinity of various ATP and ADP analogues. In the absence of ssDNA, the ATPase activity is low: ssDNA activation of ATPase activity results in 50- to 100-fold increase in k_{cat} (Table 1a).

Figure 2 (inset) shows examples for the initial time courses of ATP hydrolysis as ATP concentration varies in the presence of a DNA substrate dT_{30}. The main panel shows the rate as a function of nucleotide concentration, giving a K_m value of 3.5 μM for ATP and a k_{cat} of 16.9 s^{-1}. This value of K_m differs from that previously reported,[11] possibly because the previous assay used a coupled enzyme assay with less sensitivity and more prone to interference from reagents. Those factors can lead to difficulties getting the couple enzyme reactions fast. The fluorescent nucleotide analogue mantATP gave similar values: K_m is 2.6 μM and k_{cat} is 17.2 s^{-1}.

This assay was also used to assess the affinity of other nucleotides as inhibitors (Table 1b). ADP binds very weakly and is hydrolyzed albeit very slowly. In

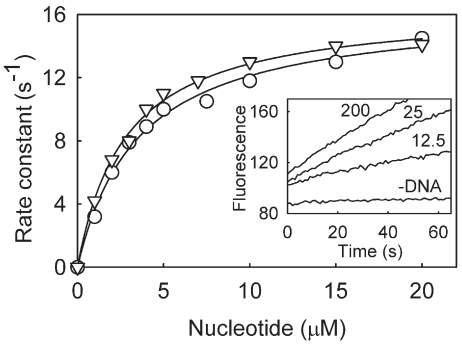

Fig. 2. Steady-state ATPase activity of PcrA. The measurements were carried out at 20 °C in a buffer containing 50 mM Tris–HCl, pH 7.5, 150 mM NaCl, and 3 mM $MgCl_2$ with 2 nM PcrA, 0.5 μM dT_{30}, 10 μM MDCC-PBP, and nucleoside triphosphate at the concentrations shown in time courses in the inset. The concentration dependence of initial rates is plotted: the circles are for ATP and triangles are for mantATP. The lines are best fits to the Michaelis–Menten equation to give a K_m of 3.5 μM and a k_{cat} of 16.9 s^{-1} for ATP and a K_m of 2.6 μM and a k_{cat} of 17.2 s^{-1} for mantATP.

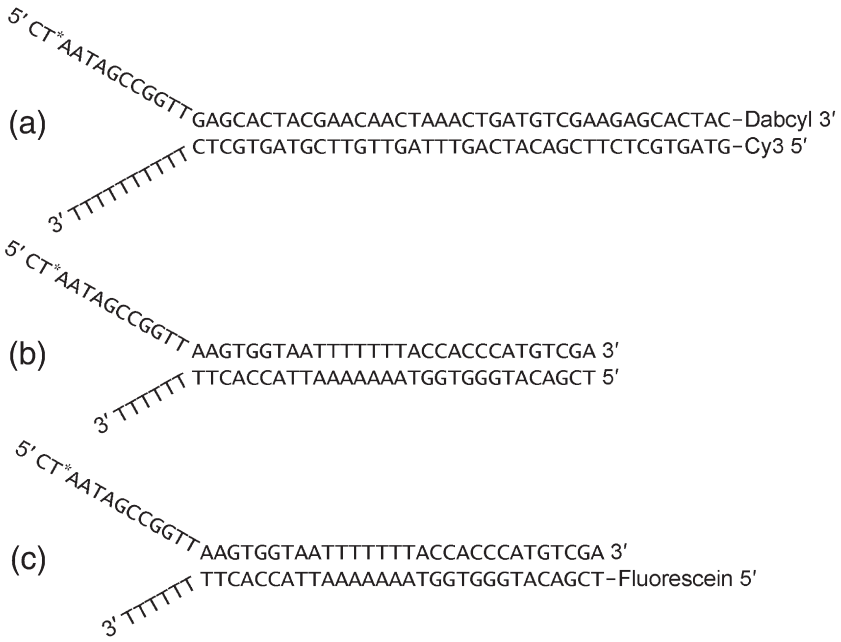

Fig. 3. Junctions used in this study. In all cases, one arm contains part of the ICRII sequence, including the RepD nick site (asterisk). The other arm contained either dT_6 or dT_{10} to allow for initial PcrA binding. (a) Junction used for translocation measurements. The double-stranded arm has 40 bp, or shorter with the appropriate sequence from 10 to 30 bp. The double-stranded arm ends with a Cy3 and Dabcyl pair, as described in the text. (b) Junction used for single-turnover ATPase kinetic measurements. The double-stranded arm (30 bp) has the ICRIII sequence. (c) Junction used for anisotropy binding measurements is as Junction b, except for a fluorescein at the end of the double-stranded arm, and both a dT_6 and a dT_{10} lower arm were used.

contrast, mantADP has a far greater affinity. The ATP analogues AMPPNP and mantAMPPNP bind weakly. In contrast, two other analogues, ATPγS and mantATPγS, bind tightly and are used here to mimic ATP binding. MantATPγS is hydrolyzed at $<0.01\ s^{-1}$ under conditions as in Table 1 and, thus, is essentially non-hydrolyzable on the time scale of measurements described here.

The measurement of ATPase rate as a function of oligonucleotide concentration (Table 1c) gave values of K_m for the DNA. This varied from 395 nM for dT_{10} to 56 nM for dT_{50}, consistent with the affinity being proportional with binding sites for PcrA, being randomly available along the oligonucleotides.[18] In addition, the k_{cat} increased with DNA length, from $5.4\ s^{-1}$ for dT_{10} to $24\ s^{-1}$ for dT_{50}, suggesting that, for these conditions, the length of DNA translocated between slow rebinding events is an important factor in determining the steady-state rate.

Assessment of mantATP as a substrate for PcrA

This fluorescent nucleotide was used as it is apparently a good substrate and provides a fairly self-consistent and complete set of rate constants. This complete set is not possible with ATP itself, using current techniques, as some steps in the ATPase cycle give no signal. Furthermore, the high affinity of mantADP for PcrA allows the ready formation of a mantADP complex. Mant ribonucleotides exist as an approximately 1:2 equilibrium of 2′- and 3′-isomers,[20] which may have different ATPase kinetics. Some measurements (phosphate transients, triphosphate binding, and steady-state ATPase rates) were also carried out with the 3′-mant-2′-deoxyATP (data not shown) to assess this possibility, which gave the same kinetics as the mixed isomer. Diphosphate dissociation kinetics were somewhat different with the single isomer and these will be described.

The above kinetic data suggest that, apart from the higher affinity of mantADP, mantATP is a reasonable ATP mimic, but in order to confirm this, we used a functional assay. In the presence of the replication initiator protein RepD, PcrA unwinds plasmids containing the double-stranded origin of replication *ori*D.[5] The unwinding and corresponding ATPase kinetics were measured with fluorescent oligonucleotides (Fig. 3a), which mimic part of *ori*D (ICRII), which is the site that RepD nicks and becomes covalently attached, thus facilitating PcrA loading.[21] These assays were done with the DNA labeled with Cy3:Dabcyl fluorophore and quencher pair, positioned to give a fluorescence signal when the DNA is unwound, as described previously[16,22] and shown in Fig. 3a. The length of the double-stranded region was varied from 10 to 40 bp, and for ATP, an unwinding rate of 48 bp s^{-1} and a hydrolysis rate of $36\ s^{-1}$ were determined at 30 °C, while for mantATP, these values were 21 bp s^{-1} and $25\ s^{-1}$, respectively (Supplementary Fig. 1). The slower rates with mantATP may reflect some inhibition by mantADP. These results are consistent with the structural and kinetic evidence, whereby one ATP is required for every base unwound[10,16,17] and indicate no significant mechanistic difference between the catalysis of the two nucleotides.

Adenosine nucleotide binding to the PcrA·dT_{20} complex

Because of the high hydrolysis rate of mantATP in the presence of ssDNA, binding to PcrA was isolated from hydrolysis by mantATP analogue that was only very slowly hydrolyzed with DNA. As shown above, mantATPγS is a better ATP analogue than mantAMPPNP in terms of affinity for PcrA (Table 1b). Figure 4 shows the traces for this analogue binding to PcrA·dT_{20} complex under

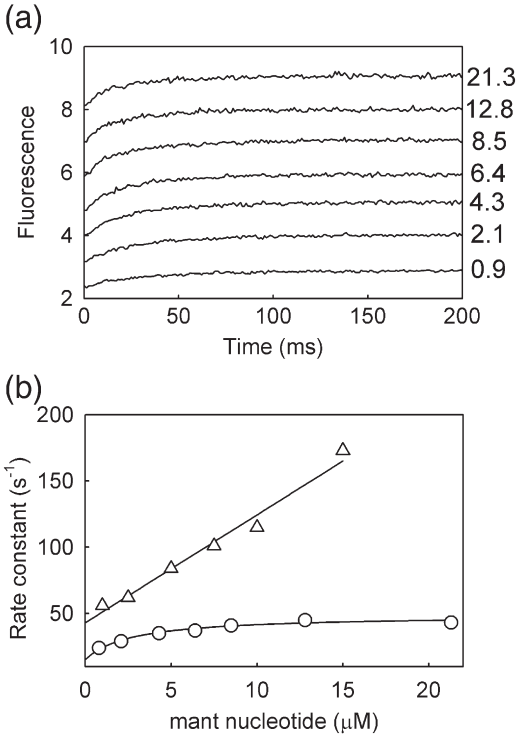

Fig. 4. Mant nucleotide binding to PcrA·dT$_{20}$. (a) MantATPγS at the micromolar concentrations shown was mixed in the stopped-flow apparatus with 0.5 μM PcrA and 2.5 μM dT$_{20}$ under the same conditions as Fig. 2. The fluorescence signal (arbitrary scale) was measured by exciting tryptophan at 290 nm and measuring the FRET to mant. Traces shown are typically an average of three individual ones and are offset for clarity. (b) mantATP (triangles) and mantATPγS (circles) binding kinetics as a function of concentration. Individual traces were fit to single exponentials, and the dependence of the rate constants on concentration was then fitted to a hyperbola or straight line, as shown. The points shown are averages of at least four measurements. The fit for mantATPγS gives $1/K_1$ as 2.7 μM, k_{-2} as 15 s^{-1}, and k_{+2} as 34 s^{-1}. The fit for mantATP gives a slope of 8.1 μM^{-1} s^{-1} and an intercept of 43 s^{-1}.

pseudo-first-order conditions: mantATPγS is in large excess over the protein. The concentration dependence of the observed rates fit well to a hyperbola. A simple model to accommodate this is a two-step binding with the first step being rapid and the second step having the predominant fluorescence change, as shown in the scheme (Fig. 1b). The fit gives $1/K_{1a}$ as 2.7 μM, k_{-1b} as 15 s^{-1}, and k_{+1b} as 34 s^{-1}, giving an overall K_d $[1/K_{1a}(1+K_{1b})]$ of 1.2 μM, similar to the value obtained from the steady-state inhibition measurement (Table 1b). Measurements were done here by exciting Trp and measuring the Förster resonance energy transfer (FRET) to mant, but the fact that the rate constants show a hyperbolic dependence on concentration suggests that the fluorescence change is not solely due to FRET in this case.

The association of mantATP to PcrA·dT$_{20}$ was also measured with excess mantATP (Fig. 4b). There was a single phase increase (not shown) with amplitudes similar to the mantATPγS binding measurement but with a linear relationship between the observed rate constants and nucleotide concentration. The slope gives a second-order association rate constant of 8.1 μM^{-1} s^{-1}. These data for mantATP binding to PcrA·dT$_{20}$ fit a model with single step binding, as described above, but now, hydrolysis needs to be included to interpret the data. The intercept with the ordinate (43 s^{-1}) is a sum of rate constants controlling breakdown of the bound mantATP, which include both its dissociation and hydrolysis leading to dissociation as the diphosphate. These data suggest that the sulfur substitution in ATP makes a large change in the parameters controlling binding: for example, mantATP may have qualitatively similar binding mechanism to mantATPγS, but the second step is so fast as to be experimentally inaccessible.

Experiments with an excess of PcrA·dT$_{20}$ over mantATP were also carried out (Fig. 5a), which allow a direct comparison with the single-turnover experiments measuring hydrolysis and P$_i$ release, described below. As with the traces using excess nucleotide, there was an initial increase in fluorescence, with a linear relationship between the ob-

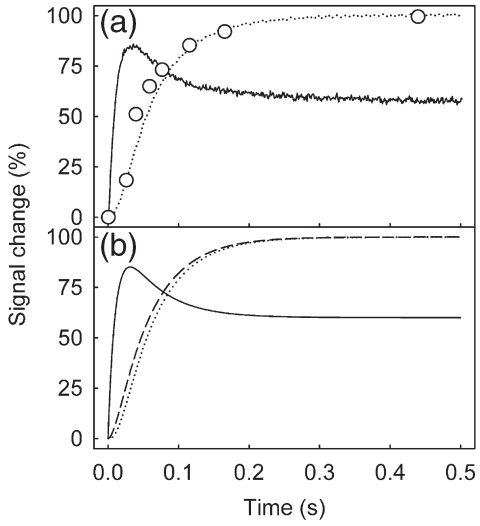

Fig. 5. Kinetic measurements with mantATP on mixing with excess of PcrA and dT$_{20}$: binding, hydrolysis, and P$_i$ release. The concentrations for all experiments were 2 μM mantATP, 8 μM PcrA, and 16 μM dT$_{20}$ under the same conditions as Fig. 2. (a) Time course of mant fluorescence, mantADP formation, and P$_i$ release. The mant fluorescence (continuous line) is the average of two traces. The amplitude of the fluorescence maximum is arbitrary and, for clarity, is set to that calculated from the simulation (below). The circles represent single time points for a quenched-flow measurement of mantADP formation. P$_i$-release kinetics (dotted line—average of three traces) were measured for the same mixture but also containing 10 μM MDCC-PBP. See Materials and Methods for details of each procedure. (b) Simulation of this time course, based upon a global model for a single turnover of ATP as described in the text, with mant fluorescence (continuous line), mantADP formation (broken line), and P$_i$ release (dotted line).

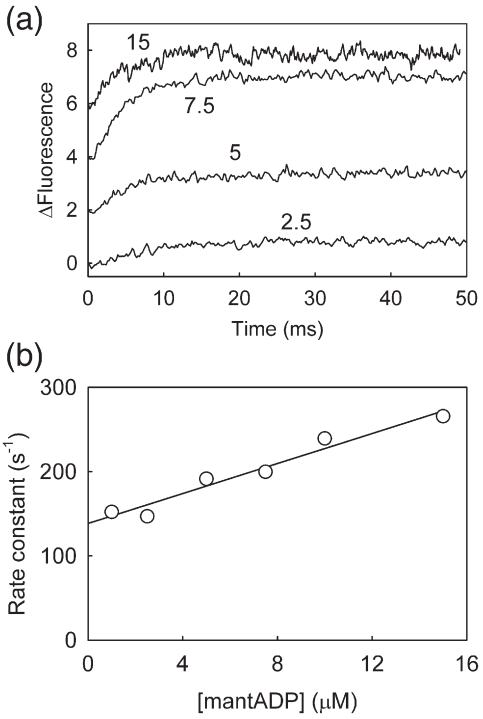

Fig. 6. MantADP binding kinetics to PcrA·dT_{20}. (a) MantADP at the micromolar concentrations shown were mixed in the stopped-flow apparatus with 0.5 μM PcrA and 2.5 μM dT_{20} under the same conditions as Fig. 2. Traces shown are typically an average of three individual ones. Traces were fitted to single exponentials, and the points shown are the average of at least three measurements. (b) Rate constants as a function of concentration and the best linear fit give a slope of 8.8 μM^{-1} s^{-1} and an intercept of 138 s^{-1}. In order to relate these data to the dissociation kinetics of mantADP, potentially occurring in two steps, we simulated this graph using two steps with reverse rate constants of 210 and 40 s^{-1} and a rate-limiting association rate constant of 10 μM^{-1} s^{-1} (representing an average value). The resulting curves were fitted to single exponentials for different concentrations of protein. This, in turn, gave an intercept of ~160 s^{-1}, similar to that obtained experimentally.

served rate and PcrA·dT_{20} concentration giving a second-order rate constant of 9.6 μM^{-1} s^{-1} for binding. As described above, interpretation of the ordinate intercept is likely to be complex. Unlike the previous measurements, the initial increase in fluorescence is followed by a smaller (~30%), slow decrease with a rate of 10 s^{-1}, which is independent of PcrA concentration. Free mantATP and mantADP have similar, low fluorescence intensities, and the second decrease phase could reflect partial dissociation of the diphosphate following hydrolysis, a transition to a lower fluorescence state, such as following cleavage, or a combination of these.

In order to aid interpretation, we also recorded anisotropy measurements under these conditions (Supplementary Fig. 2a). Anisotropy reflects the rotational correlation time of the fluorophore and that, in turn, may reflect the molecular mass to some extent. Thus, it would be expected that the main increase in anisotropy would be on binding of mant nucleotides to the protein. The fact that the second phase of anisotropy is only a small decrease is consistent with this phase representing a process following mantATP binding but before mantADP release, which would return anisotropy to the initial value. Alternatively, the second phase could represent a small equilibrium level of mantADP release, albeit less than that expected from the value of K_i for mantADP (9.5 μM, Table 1b) and the concentration of PcrA in this experiment (8 μM). This is addressed further in the modeling, described later.

Hydrolysis step and phosphate release

Quenched-flow measurements allow the formation of ADP to be monitored with high time resolution. In practice, mantATP was used as substrate to allow the use of fluorescence detection and also to conform to other measurements using this analogue. MantATP was rapidly mixed with PcrA·dT_{20}, and the reaction mix was quenched in acid to obtain individual time points for the extent of mantADP formation. Following quenching, the mix was analyzed by HPLC to separate and quantify mantATP and mantADP. This gives the time course of mantADP formation as in Fig. 5a but does not distinguish between protein-bound nucleotide and that free in solution. Figure 5a shows mantATP binding for these conditions and demonstrates that nucleotide binding is likely to be fast compared with bond cleavage. Furthermore, the decrease in fluorescence has similar kinetics to the quenched-flow measurement.

The kinetics of P_i release were measured using the phosphate biosensor MDCC-PBP under similar conditions. Fitting the trace gave rate constants of 90 s^{-1} for the lag and 18 s^{-1} for the fluorescence rise. This trace has a similar time course to the mantADP formation from the quenched-flow measurement,

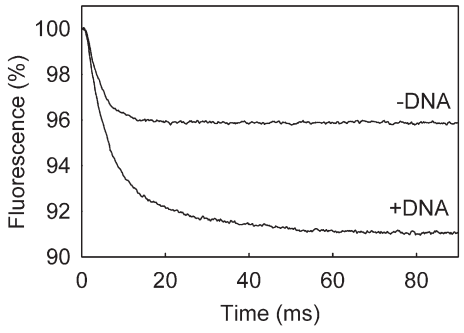

Fig. 7. MantADP release kinetics from PcrA·dT_{20}; 20 μM PcrA and 20 μM dT_{20} were premixed with 10 μM mantADP before rapid mixing with 200 μM ATP under the same conditions as Fig. 2. The trace in the absence of DNA is also shown. The traces are the average of three traces following mant fluorescence with time. In the absence of DNA, the trace was fitted to a single exponential with a rate constant of 190 s^{-1}. In the presence of DNA, the traces were fitted to a double exponential with rate constants of 215 s^{-1} for the large phase and 40 s^{-1} for the smaller decrease in fluorescence. Rate constants were independent of ATP concentration in the range of 200–600 μM.

suggesting that P_i is released rapidly following hydrolysis; that is, step 3 is fast compared with step 2 in the reaction scheme of Fig. 1a.

MantADP binding

Figure 6 shows traces for mantADP binding to PcrA·dT_{20} complex under pseudo-first-order conditions: mantADP is in large excess over protein. There is a linear dependence between observed rate constant and mantADP concentration with a second-order rate constant of 8.8 μM^{-1} s^{-1}, and the intercept, corresponding to mantADP release, was 140 s^{-1}. Measurements were also done with excess PcrA·dT_{20} over a small concentration range (Supplementary Fig. 2c). In this case, the second-order rate constant was 11 μM^{-1} s^{-1} and the intercept was 140 s^{-1}.

MantADP dissociation

PcrA·dT_{20} was premixed with mantADP and then mixed rapidly with excess ATP in a stopped-flow apparatus. The ATP acts as a trap for dissociated PcrA. A large and rapid decrease in fluorescence, 215 s^{-1}, was observed, followed by a slower phase with a rate of 40 s^{-1} (Fig. 7). Modeling, described in Fig. 6, suggests that a two-step mechanism with these rate constants is consistent with the intercept (140 s^{-1}) in the association kinetics concentration dependence described above. Measurements with 3′-mant-2′-deoxyADP gave somewhat different kinetics: 100 s^{-1} and 10 s^{-1}, suggesting that diphosphate release may be the one process in which the mant isomers differ.

Oxygen exchange measurements

Exchange measurements were done using oxygen-18 labeling in order to get information about the reverse of cleavage (step 2, Fig. 1a). Intermediate exchange can occur between terminal oxygens of the nucleotide and water during hydrolysis. Medium exchange can occur between ($^{18}O_4$)P_i and water, when the ATPase is incubated with ADP (or mantADP). The rationale for these exchanges and the analysis of P_i on a mass spectrometer have been described previously.[23,24] In this case, no exchange was observed for either type of experiment; thus, no measurable reversal of the cleavage step occurs. Within the error of the measurement, this means that $k_{+3}/k_{-2}>90$. This supports the idea that the cleavage step is essentially irreversible and followed by rapid P_i release.

Modeling

A model of the ATPase cycle was based on the scheme in Fig. 1a, which has a single step each for mantATP binding, hydrolysis, P_i release, and mantADP release. P_i release is irreversible in the model. It is assumed that the fluorescence of different protein-bound mant species is the same. The results for the global fit (Fig. 5b) gave mantATP binding at 9 μM^{-1} s^{-1} and hydrolysis at 20 s^{-1}; P_i release is fast (>130 s^{-1}) and K_d for mantADP is 6.5 μM. The rate constants for steps in the ATPase cycle with ssDNA are summarized in Table 2. This suggests a tighter binding than previous measurements but is consistent with an equilibrium of bound and free mantADP at this PcrA concentration. The single-turnover experiments were also carried out at 6 and 4 μM PcrA·dT_{20} using 2 μM mantATP and the parameters for the model fit well to these traces, including accounting for the size of the decrease in the mantATP fluorescence traces (Supplementary Fig. 2b). The corresponding ATPase measurement[17] with mantATP under these conditions gave a rate of 19 s^{-1} during the translocation phase, which is very similar to the hydrolysis rate constant obtained in the single-turnover measurements.

Measurements in the absence of DNA

As already mentioned, the presence of ssDNA leads to a 100-fold increase in ATPase activity in a steady-state assay. Measurements were carried out in the absence of DNA substrate to investigate what steps in the ATPase cycle are affected. Association measurements with excess mantATPγS gave qualitatively similar results to those with ssDNA: there is a hyperbolic relationship (data not shown) with best fit $1/K_{1a}=4.4$ μM, $k_{-1b}=13$ s^{-1}, and $k_{+1b}=10$ s^{-1}. With mantATP, there is a linear relationship with concentration (Supplementary Fig. 3a), giving rate constants from the gradient, 2.5 μM^{-1} s^{-1}, and intercept, 13.3 s^{-1}. This results in K_d being 5.3 μM.

The corresponding measurements with an excess of PcrA over mantATP were also carried out in the absence of DNA (Supplementary Fig. 3b, inset), but the same conditions as for the measurement with ssDNA were used (Fig. 5a). For PcrA binding to mantATP, a single, rapid increase in fluorescence is observed with no subsequent decrease in fluorescence within the time scale of measurements. The hydrolysis time course, measured by manual quench, is very slow and similar to that obtained for P_i release (Supplementary Fig. 3b). In the same

Table 2. Summary of individual rate constants for the hydrolysis cycle of mantATP at 20 °C

	Rate constants	
Step	dT_{20}	−DNA
k_{+1} (μM^{-1} s^{-1})	8.1	2.5
k_{-1} (s^{-1})	20	13
k_{+2} (s^{-1})	19.5	0.01
k_{-2}	n.d.	n.d.
k_{+3} (s^{-1})	>130	>1
k_{-3}	n.d.	n.d.
k_{+4} (s^{-1})	138	190
k_{-4} (μM^{-1} s^{-1})	8.8	9

Values for k_{+1}, k_{+4}, and k_{-4} were calculated from pseudo-first-order experiments, while k_{-1}, k_{+2}, and k_{+3} were taken from simulation of the single-turnover measurements to the model of the ATPase cycle in Fig. 1a.

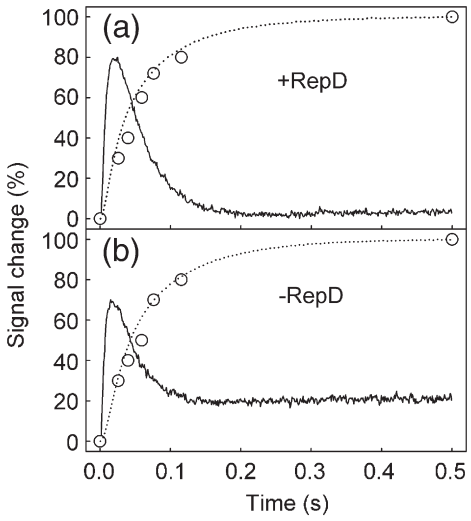

Fig. 8. Kinetic measurements with mantATP on mixing with excess of PcrA and the *ori*D–model junction in the presence and absence of RepD: binding, hydrolysis, and P_i release. Experimental conditions were 8 μM PcrA, 8 μM DNA junction, 10 μM RepD, and 2 μM mantATP at 30 °C in a buffer containing 50 mM Tris–HCl, pH 7.5, 200 mM KCl, 10 mM $MgCl_2$, 1 mM EDTA, and 10% (v/v) ethanediol. Time course of mant fluorescence (continuous line), mantADP formation (circles), and P_i release (dotted line). Measurements with RepD present (a) and absent (b).

way as with the measurements in the presence of ssDNA, the ATPase model was applied to determine the rate constants. This gives a binding rate constant of 5 μM^{-1} s^{-1}, hydrolysis at 0.01 s^{-1}, and P_i release at >1 s^{-1}.

Measurements of mantADP binding with an excess of nucleotide were not possible due to a poor signal. However, these were possible with an excess of PcrA. Traces were fitted to a single exponential (Supplementary Fig. 3c), and there is a linear relationship with concentration, giving a rate constant from the slope of 9.8 μM^{-1} s^{-1} and an intercept of 190 s^{-1}. For measurements of mantADP dissociation, there is a rapid decrease in fluorescence with a rate of 190 s^{-1}, similar to that with ssDNA, but the second phase is absent (Fig. 7). All oxygen exchange experiments, carried out in the absence of DNA, showed no exchange; hence, the cleavage step is irreversible (k_{+3}/k_{-2}>90), assuming free rotation of the P_i in the catalytic site.

The rate constants obtained in the absence of DNA are summarized in Table 2.

Measurements in the presence of RepD

In order for PcrA to act as a processive helicase, other protein factors are required, such as the plasmid replication initiator RepD. To investigate whether interaction with RepD affects ATPase cycle kinetics, measurements were made using a Y-shaped DNA junction (Fig. 3b) to which both proteins can bind to form an initiation complex that can then separate the dsDNA region.[16] This junction contains the ICRIII sequence in a double strand for tight binding of RepD, part of ICRII on one single-strand arm for nicking and covalent attachment of RepD, and a short single-strand arm (six nucleotides) for PcrA to bind. This short ssDNA arm was used to ensure that only one PcrA molecule binds per junction. Before measurements were taken, RepD was incubated with the DNA junction to allow nicking to occur. PcrA will then bind to the junction and unwind the duplex DNA in the presence of mantATP. Measurements were done at 30 °C in a buffer containing 50 mM Tris–HCl, pH 7.5, 200 mM KCl, 10 mM $MgCl_2$, 1 mM ethylenediaminetetraacetic acid, and 10% ethanediol to provide a direct comparison with previous work on unwinding of PcrA and RepD, particularly using similar oligonucleotide models.[16]

Fluorescence anisotropy was used to measure binding of PcrA to the adduct of RepD and the Y-shaped DNA junction (Fig. 3c), containing a fluorescein at the end of the ICRIII duplex, as previously described.[16] The K_d is 72 nM but increased to 140 nM in the absence of RepD. In either case, these data suggest that the complex between PcrA and DNA is formed quantitatively under the conditions of experiments described below.

The single-turnover measurements (excess protein over nucleotide) were carried out, equivalent to those described above with dT_{20} (Fig. 5). Mant fluorescence, quenched flow, and P_i-release traces in the presence of RepD are shown in Fig. 8a. Qualitatively, rather similar kinetics are observed to those with dT_{20}, albeit the latter are at 20 °C. A rapid increase in mant fluorescence occurs upon binding nucleotide before a slower decrease in fluorescence with similar kinetics to hydrolysis and P_i release. Unlike previous measurements, complete dissociation of mant nucleotide is observed. This indicates a considerably weaker affinity for mantADP than the ssDNA measurements. P_i release is rapid following cleavage, showing again that hydrolysis is likely to be rate limiting. In the absence of RepD, the observed kinetics were similar, but mantADP does not fully dissociate (Fig. 8b). The parameters obtained by fitting the ATPase model, as used with ssDNA, are shown in Table 3, and the modeled traces are in Supplementary Fig. 4.

The hydrolysis step has a rate constant of 24 s^{-1}, comparable to the ATPase rate with mantATP

Table 3. Summary of kinetic parameters for the PcrA ATPase cycle obtained for the *ori*D–model junction with or without RepD loaded at 30 °C

	Rate constants	
Step	+RepD	−RepD
k_{+1} (μM^{-1} s^{-1})	20	20
k_{-1} (s^{-1})	10	45
k_{+2} (s^{-1})	24	24
k_{+3} (s^{-1})	>300	>300
mantADP K_d (μM)	>100	50

Values were obtained from simulating the data in Fig. 8, as described in the text with k_{-2} and k_{-3} set to zero.

during unwinding of 25 s^{-1} for these conditions. The experimental trace for P_i in the presence of RepD shows a small slow phase. This may occur due to heterogeneity in the PcrA activity. Measurements were taken with different DNA junctions whereby the length of ssDNA overhang, for PcrA binding, was varied. With a 10-nucleotide arm, both the decrease in mant fluorescence and P_i-release traces were biphasic (data not shown). The slower component had a larger amplitude than that with the 6-nucleotide arm shown in Fig. 8. One possible cause of this biphasic signal is the different binding positions of PcrA, which results in different populations of ATPase activity. Reducing the length of this arm limits the variable positions of PcrA binding.

With transient, single-turnover measurements for a system that normally does repeated turnovers, there is always a concern that the first turnover is not representative. In this case, there might be a possibility that for the first (or first few) ATPase cycles, the helicase may not be in a fully active state in terms of interaction with RepD and effective duplex unwinding. In order to test for this, a double-mix stopped-flow experiment was done, in which PcrA, RepD, and DNA were first mixed with a 3-fold excess ATP. This takes advantage of the weak binding of ADP, so that this product should not interfere with the subsequent mantATP binding. After various time periods to allow hydrolysis and nucleotide release, the solution was mixed with mantATP and fluorescence followed with time. The kinetics from this double-mix experiment (Supplementary Fig. 5) were identical with those already determined for the first turnover (Fig. 8a). This suggests that the first and subsequent turnovers are similar.

Measurements with ATP and ADP

Where possible, individual ATPase steps were investigated using unmodified nucleotides for PcrA in the presence of dT_{20}. Although the small changes in tryptophan fluorescence were not useful to examine binding of ATP to PcrA·dT_{20}, this signal could be used with PcrA alone. Using the same pseudo-first-order condition as with mantATP, a binding rate constant of 4.5 μM^{-1} s^{-1} and dissociation rate constant of 22 s^{-1} were measured (data not shown). These rate constants are slightly higher than those for mantATP binding to PcrA alone but the K_d remains 5 μM.

A competition experiment was carried out between mantATP and ATP in order to determine a second-order binding rate constant for ATP with PcrA·dT_{20} (Fig. 9).[25] Pseudo-first-order conditions were used as above, but mantATP was fixed at 5 μM as the ATP concentration varied. The slope of the plot of the observed rate constant against ATP concentration gives the rate constant for association of ATP to be 8 μM^{-1} s^{-1}, similar to that of mantATP. A dissociation rate constant cannot be accurately determined from intercepts for this type of measurement, as this intercept includes the rate constant of mantATP binding, introducing a large error.

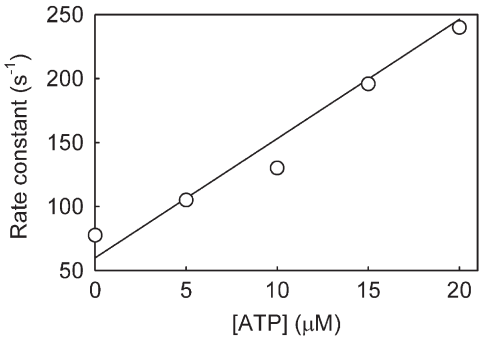

Fig. 9. ATP binding kinetics to PcrA·dT_{20}. ATP at micromolar concentrations shown and 5 μM mantATP were mixed in the stopped-flow apparatus with 0.5 μM PcrA and 2.5 μM dT_{20} under the same conditions as Fig. 2. Traces were fitted to single exponentials, and the points shown are the average of at least three measurements. Rate constants as a function of concentration and the best linear fit give a second-order rate constant for ATP binding of 8 μM^{-1} s^{-1}.

The single-turnover, P_i-release measurement was also carried out with ATP (Supplementary Fig. 6). The ATPase model for the single-turnover measurements was applied to fit the data. From this, a hydrolysis rate constant of 36 s^{-1} was obtained. The ATPase rate during ssDNA translocation was measured, as described previously,[17] giving a rate of 46 s^{-1} (data not shown). The difference between ATPase rate and the P_i-release rate may be due to incomplete PcrA·dT_{20}·ATP complex formation for these single-turnover conditions because of the somewhat lower affinity of ATP compared to mantATP.

Oxygen exchange experiments with ATP/ADP also showed no exchange, putting the limits of $k_{+3}/k_{-2}>90$. ADP has a very weak affinity for PcrA: K_i is >400 μM from steady-state ATPase activity measurements (Table 1); ADP binding or dissociation kinetics were not measured.

Discussion

The main sets of rate constants coming out of this work are summarized in Tables 2 and 3. In order to relate the ATPase cycle to previous biochemical data on PcrA, particularly with ssDNA and with RepD, this resulted in two sets of conditions. For reasons explained earlier, mantATP was the main nucleotide used to obtain self-consistent sets of rate constants. In most ways, mantATP is an excellent analogue of ATP. Most rate constants measured and translocation rates are similar for the two nucleotides. The only large change is at the diphosphate interaction: mantADP binds much tighter than ADP. This phenomenon of a large change with diphosphate release has been reported for other ATPases with mantADP and other ribose-modified nucleotides.[26–28] It seems likely that in such cases, the mant group may interact with the protein surface in the diphosphate case. Surprisingly with

PcrA, this does not produce a fluorescence intensity much different from the bound triphosphate.

The single-turnover measurements of mant fluorescence, mantADP formation, and P_i measurement, shown in Figs. 5 and 8 and Supplementary Fig. 2, provide a ready visual comparison of the ATP kinetics, and these were the main focus of comparing complexes of PcrA under different conditions, such as the type of DNA.

The most detailed measurements were done with PcrA bound to ssDNA, and thus, we will first examine the ATPase cycle in that complex. MantATP binding has similar second-order binding rate constant to that found with a variety of other ATPases but well below what might be expected for diffusion control. MantATPγS shows a hyperbolic dependence of rate on concentration, suggesting two-step binding, normally considered as formation of a collision complex, followed by some rearrangement/conformation change to produce the "productive complex", although in the case of this analogue, the cleavage step is severely disrupted. It is possible that the same transition occurs with mantATP but is not seen experimentally because of its high rate of cleavage. The cleavage step is likely to be rate limiting and irreversible at typical triphosphate concentrations. This suggests that the bound triphosphate complex is the most populated intermediate during the cycle. Phosphate release is rapid, and we can estimate only an approximate lower limit for its rate constant. MantADP release is the most enigmatic. ADP binds very weakly to PcrA (Table 1), although mantADP is quite tight. MantADP binding kinetics are approximately similar to those of mantATP. Dissociation kinetics of mantADP from PcrA differs depending on whether or not DNA is present. In the absence of DNA, a single rapid phase is observed (Fig. 7). A similar phase is observed when PcrA is bound to ssDNA or to the DNA junction, but in addition, there is a slower phase, suggesting that there may be a two-step process for diphosphate release, as shown in Fig. 1c. If it were the case that both rate constants are on the ATPase pathway, k_{+4a} is 215 s^{-1} and k_{+4b} is 40 s^{-1}. A rate constant of 40 s^{-1} would give a calculated K_d of 4.5 μM, similar to that obtained from the modeling (6.5 μM) but 2-fold tighter than the value obtained from steady-state measurements, although that final value may not be exactly comparable as the PcrA is not in a single environment. The 40 s^{-1} rate constant is not much faster than cleavage and would lead to bound diphosphate being a major intermediate.

DNA accelerates the cleavage step by more than 3 orders of magnitude, and this step may be the main one affected by interaction with DNA. However, we could not exclude a very small contamination by DNA producing this slow ATP cleavage. This is consistent with structural information relating to conformation changes in the ATP binding site,[10,13] such as movement of an arginine (R287) to near the γ-phosphate and movement of K37 out of the Mg site on binding DNA.

RepD has a dramatic effect on increasing the processivity of PcrA with dsDNA,[5,16,29] although the way this is achieved is not yet understood. The experimental design of short single-strand overhang and equimolar DNA and PcrA would favor a single PcrA monomer being active in this case. In principle, RepD could maintain PcrA binding to the DNA, such as by decreasing the dissociation rate. This could be a direct effect of interaction between these two proteins in such a way as the complex remains tightly bound. This, in turn, could be either due to the geometry of the complex, such as DNA going through a hole in the protein complex, or due to RepD having a high affinity for DNA and for PcrA. Note that the covalent linkage of RepD to the DNA is at the 5′-end and, after some strand separation, is distant in DNA sequence from the site of unwinding. RepD could also maintain PcrA binding to DNA indirectly by causing a conformation change in PcrA that changes its enzymic activity. However, the ATPase data presented here show no large changes in the cycle produced by the presence of RepD, except for the weakened affinity of mantADP. A high K_d is induced in part by the DNA junction in the absence of RepD, and in either case, the weak binding and small signal made measurements of mantADP kinetics inaccessible.

Several pieces of evidence suggest that PcrA interacts fully with RepD on binding; hence, the ATPase cycle probed here represents the fully active complex. Firstly, the double-mixing experiment, allowing a few turnovers with ATP to occur before measurement with mantATP begins, shows no difference from a single turnover. Secondly, it was demonstrated previously that, even in the absence of ATP, RepD enhances the affinity of PcrA for an *ori*D–model junction, similar to the one used here (Fig. 3c), by an order of magnitude.[16] Finally, the kinetics of the ATPase cycle are consistent with the unwinding rate observed with mantATP for these conditions (25 s^{-1}).

The results here suggest that RepD interaction has little effect on the ATPase cycle and that it is likely to have its effect on processivity by increasing PcrA affinity for the RepD–DNA junction where it acts. Presumably, that needs to be associated with a large decrease in the dissociation rate of PcrA while translocation is occurring.

The ATPase kinetics have been investigated in detail for rather few helicases, given the wide variation in this family. The nucleotide binding and hydrolysis kinetics were measured for both monomer and dimer of a superfamily 1 helicase, Rep.[30–32] Despite the structural similarities with PcrA, the ATPase mechanism shows marked differences. In the active dimer, binding occurs in two steps and a rate-limiting isomerization step precedes product release. The ATPase mechanism in this instance is complicated due to the two ATPase sites of the dimeric Rep and communication between the two sites. The ATPase mechanism of a superfamily 2, DEAD-box RNA helicase, DbpA, has also been elucidated.[33] This helicase is likely to have a two-

step ADP release, and the slowest steps are cleavage and P_i release, with significant reversibility in the cleavage step. In each case, the ATPase activity is greatly enhanced by DNA or RNA substrates, depending on the type of helicase. The differences in mechanisms highlight the diversity among helicases, both within and between superfamilies. However, with so few cases elucidated, it would be difficult to generalize any relationship between classes of helicase and mechanism. Indeed, factors such as processivity and translocation rate, required for particular physiological roles, may also be significant in determining what ATPase mechanism may be appropriate.

In summary, the elucidation of the ATPase cycle has shown a remarkably simple mechanism with a rate-limiting and essentially irreversible cleavage step, greatly accelerated by bound DNA and presumably corresponding to the major transition between structural states.[34] This would fit in with the idea that the translocation is essentially unidirectional. There is tentative evidence for two-step diphosphate release, but generally, this helicase exemplifies a very different ATPase mechanism from myosins and their activation by actin.[35–37] Thus, the two major states present during translocation are the triphosphate and diphosphate states: the ADP·P_i state has an extremely low population. With PcrA, there is no need for the ATPase kinetics to be tuned to enable dissociation of helicase from DNA each cycle, followed by finding the next target on its track: that is necessary for motors such as myosins with actin track. The "hand-over-hand" mechanism[12] ensures that the next bit of the track is always on hand! While RepD helps maintain PcrA at the junction, the strands are pulled apart through relatively simple conformation changes presumably more-or-less coinciding with steps on the hydrolysis pathway. Currently, there is little evidence that RepD binds directly to PcrA, but such interaction could be via the IIB subdomain of the latter, well away from the ATP site, but close to the region affected by dsDNA binding.

Materials and Methods

Materials

PcrA from *B. stearothermophilus* was expressed and purified as described previously.[16,38] Coumarin-labeled phosphate protein (MDCC-PBP) was prepared as described previously.[19] RepD from *Staphylococcus aureus* was prepared as described previously.[16,21]

($^{18}O_4$)P_i and (γ-$^{18}O_3$)ATP were synthesized from (^{18}O)water (97% enriched) as described previously.[39] MantATP, mantADP, and mantATPγS were synthesized from their parent nucleotides by a slight modification of the method of Hiratsuka.[40,41] Labeled and unlabeled oligonucleotides were from Eurogentec Ltd. (Southampton, UK). In order to make the DNA substrates, we mixed oligonucleotides generally at equimolar concentrations at 500 μM in a volume of 200 μl in a buffer containing 50 mM Tris–HCl, pH 7.5, 200 mM KCl, 10 mM $MgCl_2$, and 1 mM EDTA. Cy3- and Dabcyl-labeled oligonucleotides, defined in Fig. 3a, were mixed at a 5:6 molar ratio in order to minimize free Cy3 (i.e., not paired and therefore quenched by Dabcyl). After mixing, oligonucleotides were heated to 95 °C for 5 min, before cooling to room temperature for 2 h, and were then stored frozen at −20 °C. All other biochemical reagents were from Sigma, UK.

Oxygen exchange measurements

For intermediate exchange during ATP hydrolysis, 0.5 μM PcrA and 1 mM (γ-$^{18}O_3$)ATP were incubated for 10 min (+1 μM dT_{20}) or 20 min (−DNA). For measurements with (^{18}O)water, 1 mM ATP or mantATP was made up in the appropriate buffer using unlabeled water. These solutions were lyophilized and then redissolved in the same volume of (^{18}O)water; 10 nM PcrA and 0 or 0.5 μM dT_{20} were then added and samples were incubated for 15 min (+DNA) or 30 min (−DNA). To determine the isotopic enrichment of these solutions, 10 μL of each was incubated for 1 h with 1 mg PCl_5, which is hydrolyzed to phosphate and can then be analyzed as below. The incubation samples were then diluted with unlabeled water prior to analysis.

For medium exchange measurements (P_i–water), 5 μM PcrA and 30 μM ADP or mantADP were incubated with 0.5 mM ($^{18}O_4$)KH_2PO_4 for 5 and 20 h. The starting enrichment was calculated from the ^{18}O distribution determined from the control incubation in the absence of protein. There was almost no exchange in this control, and thus, this distribution is taken as that of the starting ($^{18}O_4$)P_i.

P_i was analyzed for distribution of different ^{18}O-labeled species on a mass spectrometer as described previously,[23] with modifications.[24] MDCC-PBP detection was used for all samples with no radioactive tracers.

Quenched-flow measurements

These were carried out using a HiTech RQF-63 apparatus with different length loops and flow rates to age reactions before quenching. Reactions (in a total volume of 300 μL) were quenched using 10% perchloric acid (150 μL) and then partially neutralized to pH ~4 using 4 M sodium acetate (70 μL). Samples were then analyzed by HPLC using a Whatman SAX Partisphere column (0.4 cm×10 cm), eluting at 1 mL min^{-1} with 80% (v/v) 0.3 M $(NH_4)_2HPO_4$, adjusted to pH 4.0 by HCl, and 20% methanol. Mant fluorescence was monitored with a Waters 2475 fluorescence detector, connected to the HPLC column, using an excitation wavelength of 366 nm and detecting emission at 440 nm. Peaks for mantADP and mantATP were integrated using the Waters Empower software.

Optical measurements

Stopped-flow experiments were carried out in a HiTech SF61MX apparatus (TgK Ltd., Bradford-on-Avon, UK) with a mercury–xenon light source and HiTech IS-2 software. For MDCC-PBP fluorescence, the excitation wavelength used was 436 nm, and a 455-nm cutoff filter (Schott glass) was used to collect emitted light. For measurements with PcrA in excess over mant nucleotide, 366 nm was used to excite and a 400-nm cutoff filter (Schott glass) was used to collect light, for direct excitation. For conditions with excess mant nucleotide, direct mant excitation gave a high background signal.

Therefore, the fluorescence signal was monitored by exciting tryptophan at 290 nm and measuring FRET to mant, using a 400-nm cutoff filter. Measurements of Cy3 fluorescence used 547 nm excitation and a 570-nm cutoff filter. Anisotropy was measured with the instrument in the "T" format, allowing simultaneous acquisition of horizontal ($I_{//}$) and perpendicular ($I_{\perp}$) components. This enabled anisotropy $(I_{//}-I_{\perp})/(I_{//}+2I_{\perp})$ and intensity $(I_{//}+2I_{\perp})$ to be calculated from the same set of data.[25] Double-mixing experiments were carried using the same stopped-flow system, allowing rapid mixing of two solutions, followed by specific time periods prior to mixing with a third solution, which triggers data acquisition.

In experiments described, the quoted concentrations are those in the mixing chamber except where stated. Data were fitted to theoretical curves using the HiTech software or Grafit.[42] Typically, the data shown are the average of three individual traces.

Steady-state fluorescence was measured using a Cary Eclipse fluorometer with a xenon light source. Absorbance spectroscopy was carried out using a Beckman DU640 spectrophotometer.

Fluorescence anisotropy titrations were performed at 30 °C using an ISS PC1 photon counting spectrofluorometer with a xenon arc lamp. Anisotropy was calculated using the equations as described previously.[43] Observed anisotropy data were fitted to obtain dissociation constants using Grafit fitting software.[42]

Kinetic measurements

All reactions with PcrA and ssDNA were done at 20 °C in a buffer containing 50 mM Tris–HCl, pH 7.5, 150 mM NaCl, and 3 mM $MgCl_2$. The ssDNA was dT_{20} except where indicated.

Measurements of dsDNA unwinding in the presence of RepD were done at 30 °C in a buffer containing 50 mM Tris–HCl, pH 7.5, 200 mM KCl, 10 mM $MgCl_2$, 1 mM EDTA, and 10% ethanediol as described previously.[16] Control measurements of the ATPase activity using dT_{20} were carried out in order to assess the effect of changing to this buffer. The single-turnover measurements with ssDNA at 20 °C in this buffer show a 50% reduction in ATPase activity relative to 50 mM Tris–HCl, pH 7.5, 150 mM NaCl, and 3 mM $MgCl_2$. Parallel measurements were carried out in the absence of RepD in order to determine the effect of changing conditions (DNA structure, buffer, and temperature). However, it should be noted that when RepD is not bound to one arm of the junction, presumably, PcrA can bind to either arm.

Steady-state ATPase measurements were measured in a solution (60 μl) at 20 °C, containing 2 nM PcrA, 500 nM ssDNA, and 10 μM MDCC-PBP with varying nucleotide concentrations as substrate or inhibitor.

Analysis of kinetic data

Kinetic simulations were performed using Berkeley Madonna (Version 8.3).

Acknowledgements

This work was supported by the Medical Research Council, UK. We thank Dr. John Eccleston [MRC National Institute for Medical Research (NIMR), London] for help with quenched flow and helpful discussions, Jackie Hunter (NIMR) for preparing MDCC-PBP, and Gordon Reid (NIMR) for help preparing mant nucleotides.

Supplementary Data

Supplementary data associated with this article can be found, in the online version, at doi:10.1016/j.jmb.2009.07.071

References

1. Gorbalenya, A. E. & Koonin, E. V. (1993). Helicases: amino acid sequence comparisons and structure–function relationships. *Curr. Opin. Struct. Biol.* **3**, 419–429.
2. McGlynn, P. & Lloyd, R. G. (2000). Modulation of RNA polymerase by (p)ppGpp reveals a RecG-dependent mechanism for replication fork progression. *Cell*, **101**, 35–45.
3. Singleton, M. R., Dillingham, M. S. & Wigley, D. B. (2007). Structure and mechanism of helicases and nucleic acid translocases. *Annu. Rev. Biochem.* **76**, 23–50.
4. Iordanescu, S. & Bargonetti, J. (1989). *Staphylococcus aureus* chromosomal mutations that decrease efficiency of Rep utilization in replication of pT181 and related plasmids. *J. Bacteriol.* **171**, 4501–4503.
5. Soultanas, P., Dillingham, M. S., Papadopoulos, F., Phillips, S. E., Thomas, C. D. & Wigley, D. B. (1999). Plasmid replication initiator protein RepD increases the processivity of PcrA DNA helicase. *Nucleic Acids Res.* **27**, 1421–1428.
6. Niedziela-Majka, A., Chesnik, M. A., Tomko, E. J. & Lohman, T. M. (2007). *Bacillus stearothermophilus* PcrA monomer is a single-stranded DNA translocase but not a processive helicase in vitro. *J. Biol. Chem.* **282**, 27076–27085.
7. Yang, Y., Dou, S.-X., Ren, H., Wang, P.-Y., Zhang, X.-D., Qian, M. *et al.* (2008). Evidence for a functional dimeric form of the PcrA helicase in DNA unwinding. *Nucleic Acids Res.* **36**, 1976–1989.
8. Levin, M. K., Wang, Y. H. & Patel, S. S. (2004). The functional interaction of the hepatitis C virus helicase molecules is responsible for unwinding processivity. *J. Biol. Chem.* **279**, 26005–26012.
9. Byrd, A. K. & Raney, K. D. (2005). Increasing the length of the single-stranded overhang enhances unwinding of duplex DNA by bacteriophage T4 Dda helicase. *Biochemistry*, **44**, 12990–12997.
10. Velankar, S. S., Soultanas, P., Dillingham, M. S., Subramanya, H. S. & Wigley, D. B. (1999). Crystal structures of complexes of PcrA DNA helicase with a DNA substrate indicate an inchworm mechanism. *Cell*, **97**, 75–84.
11. Dillingham, M. S., Soultanas, P. & Wigley, D. B. (1999). Site-directed mutagenesis of motif III in PcrA helicase reveals a role in coupling ATP hydrolysis to strand separation. *Nucleic Acids Res.* **27**, 3310–3317.
12. Soultanas, P. & Wigley, D. B. (2000). DNA helicases: 'inching forward'. *Curr. Opin. Struct. Biol.* **10**, 124–128.
13. Subramanya, H. S., Bird, L. E., Brannigan, J. A. & Wigley, D. B. (1996). Crystal structure of DExx box DNA helicase. *Nature*, **384**, 379–383.

14. Soultanas, P., Dillingham, M., Wiley, P., Webb, M. R. & Wigley, D. B. (2000). Uncoupling DNA translocation and helicase activity in pcrA: direct evidence for an active mechanism. *EMBO J.* **19**, 3799–3810.
15. Lee, J. Y. & Yang, W. (2006). UvrD helicase unwinds DNA one base pair at a time by a two-part power stroke. *Cell*, **127**, 1349–1360.
16. Slatter, A. F., Thomas, C. D. & Webb, M. R. (2009). PcrA helicase tightly couples ATP hydrolysis to unwinding double-stranded DNA, modulated by the replication initiator protein, RepD. *Biochemistry*, **48**, 6326–6334.
17. Dillingham, M. S., Wigley, D. B. & Webb, M. R. (2000). Demonstration of unidirectional single-stranded DNA translocation by PcrA helicase: measurement of step size and translocation speed. *Biochemistry*, **39**, 205–212.
18. Dillingham, M. S., Wigley, D. B. & Webb, M. R. (2002). Direct measurement of single stranded DNA translocation by PcrA helicase using the fluorescent base analogue 2-aminopurine. *Biochemistry*, **41**, 643–651.
19. Brune, M., Hunter, J. L., Howell, S. A., Martin, S. R., Hazlett, T. L., Corrie, J. E. T. & Webb, M. R. (1998). Mechanism of inorganic phosphate interaction with phosphate binding protein from *Escherichia coli*. *Biochemistry*, **37**, 10370–10380.
20. Cremo, C. R., Neuron, J. M. & Yount, R. G. (1990). Interaction of myosin subfragment 1 with fluorescent ribose-modified nucleotides. A comparison of vanadate trapping and SH1–SH2 cross-linking. *Biochemistry*, **29**, 3309–3319.
21. Thomas, C. D., Balson, D. F. & Shaw, W. V. (1990). *In vitro* studies of the initiation of Staphylococcal plasmid replication. Specificity of RepD for its origin (*oriD*) and characterization of the RepD-*ori* tyrosyl ester intermediate. *J. Biol. Chem.* **265**, 5519–5530.
22. Martinez-Senac, M. M. & Webb, M. R. (2005). Mechanism of translocation and kinetics of DNA unwinding by the helicase RecG. *Biochemistry*, **44**, 16967–16976.
23. Hibberd, M. G., Webb, M. R., Goldman, Y. E. & Trentham, D. R. (1985). Oxygen exchange between phosphate and water accompanies calcium-regulated ATPase activity of skinned fibers from rabbit skeletal muscle. *J. Biol. Chem.* **260**, 3496–3501.
24. Phillips, R. A., Hunter, J. L., Eccleston, J. F. & Webb, M. R. (2003). The mechanism of Ras GTPase activation by neurofibromin. *Biochemistry*, **42**, 3956–3965.
25. Eccleston, J. F., Hutchinson, J. P. & White, H. D. (2001). Stopped-flow techniques. In *Protein–Ligand Interactions: Structure and Spectroscopy. A Practical Approach Series* (Harding, S. E. & Chowdry, B. Z., eds), pp. 201–237, Oxford University Press, Oxford, UK.
26. Talavera, M. A. & De La Cruz, E. M. (2005). Equilibrium and kinetic analysis of nucleotide binding to the DEAD-box RNA helicase DbpA. *Biochemistry*, **44**, 959–970.
27. Kurzawa-Goertz, S. E., Perreault-Micale, C. L., Trybus, K. M., Szent-Györgyi, A. G. & Geeves, M. A. (1998). Loop I can modulate ADP affinity, ATPase activity, and motility of different scallop myosins. Transient kinetic analysis of S1 isoforms. *Biochemistry*, **37**, 7517–7525.
28. Forgacs, E., Cartwright, S., Kovacs, M., Sakamoto, T., Sellers, J., Corrie, J. E. T. *et al.* (2006). Kinetic mechanism of a single-headed myosinV construct using a novel fluorescent ATP analogue. *Biochemistry*, **45**, 13035–13045.
29. Zhang, W., Dillingham, M. S., Thomas, C. D., Allen, S., Roberts, C. J. & Soultanas, P. (2007). Directional loading and stimulation of PcrA helicase by the replication initiator protein RepD. *J. Mol. Biol.* **371**, 336–348.
30. Moore, K. J. & Lohman, T. M. (1994). Kinetic mechanism of adenine nucleotide binding to and hydrolysis by the *Escherichia coli* Rep monomer. 1. Use of fluorescent nucleotide analogues. *Biochemistry*, **33**, 14550–14564.
31. Moore, K. J. & Lohman, T. M. (1994). Kinetic mechanism of adenine nucleotide binding to and hydrolysis by the *Escherichia coli* Rep monomer. 2. Application of a kinetic competition approach. *Biochemistry*, **33**, 14565–14578.
32. Hsieh, J., Moore, K. J. M. & Lohman, T. M. (1999). A two-site kinetic mechanism for ATP binding and hydrolysis by *E. coli* Rep helicase dimer bound to a single-stranded oligodeoxynucleotide. *J. Mol. Biol.* **288**, 255–274.
33. Henn, A., Cao, W., Hackney, D. D. & De La Cruz, E. M. (2008). The ATPase cycle mechanism of the DEAD-box rRNA helicase, DbpA. *J. Mol. Biol.* **377**, 193–205.
34. Dillingham, M. S., Soultanas, P., Wiley, P., Webb, M. R. & Wigley, D. B. (2001). Defining the roles of individual residues in the single-stranded DNA binding site of PcrA helicase. *Proc. Natl Acad. Sci. USA*, **98**, 8381–8387.
35. Hibberd, M. G. & Trentham, D. R. (1986). Relationship between chemical and mechanical events during muscular contraction. *Annu. Rev. Biophys. Biophys. Chem.* **15**, 119–161.
36. Hackney, D. D. (1996). The kinetic cycles of myosin, kinesin, and dynein. *Annu. Rev. Physiol.* **58**, 731.
37. De La Cruz, E. M. & Ostap, E. M. (2004). Relating biochemistry and function in the myosin superfamily. *Curr. Opin. Cell Biol.* **16**, 61–67.
38. Bird, L. E., Brannigan, J. A., Subramanya, H. S. & Wigley, D. B. (1998). Characterisation of *Bacillus stearothermophilus* PcrA helicase: evidence against an active rolling mechanism. *Nucleic Acids Res.* **26**, 2686–2693.
39. Webb, M. R. & Trentham, D. R. (1981). The mechanism of ATP hydrolysis catalyzed by myosin and actomyosin, using rapid reaction techniques to study oxygen exchange. *J. Biol. Chem.* **256**, 10910–10916.
40. Hiratsuka, T. (1983). New ribose-modified fluorescent analogs of adenine and guanine nucleotides available as substrates for various enzymes. *Biochim. Biophys. Acta*, **742**, 496–508.
41. Jameson, D. M. & Eccleston, J. F. (1997). Fluorescent nucleotide analogs: synthesis and applications. *Methods Enzymol.* **278**, 363–390.
42. Leatherbarrow, R. J. (2001). Grafit Version 5 Erithacus Software Ltd., Horley, UK.
43. Brownbridge, G. G., Lowe, P. N., Moore, K. J. M., Skinner, R. H. & Webb, M. R. (1993). Interaction of GTPase activating proteins (GAPs) with p21ras measured by a novel fluorescence anisotropy method. Essential role of Arg-903 of GAP in activation of GTP hydrolysis on p21ras. *J. Biol. Chem.* **268**, 10914–10919.